Acceleration of Nonradiative Charge Recombination

Reactions at Larger Distance in Kinked Donor-

Bridge-Acceptor Molecules

Samuel Johnson, ¹ Amrita Makhijani, ¹ Miu Tsuji, ¹ and Tomoyasu Mani^{1,2}*

¹ Department of Chemistry, University of Connecticut, Storrs CT 06033, United States

² Chemistry Division, Brookhaven National Laboratory, Upton NY 11973, United States

*tomoyasu.mani@uconn.edu / tmani@bnl.gov

ABSTRACT

Photoinduced electron transfer in donor-bridge-acceptor (D-B-A) molecular systems can

occur via tunneling over long distances (rDA) of well over 10 Å. We commonly observe

decreasing rates of electron transfer with increasing distances, a result of a decrease in the

electronic coupling of the donor and acceptor moiety. In the study of D-B-A molecules with

Ru(bpy)₃²⁺ as a bridge/core, Kuss-Petermann and Wenger observed the opposite trend (J. Am.

Chem. Soc. 2016, 138, 1349); a maximum rate constant of electron transfer was observed at an

intermediate electron transfer distance. Within the high-temperature limit of the classical Marcus

equation, their observation was qualitatively explained by a sharp distance dependence of outer

1

sphere (or solvent) reorganization energy, as predicted by Sutin and co-workers (J. Am. Chem. Soc. 1984, 106, 6858), and almost distance independent electronic couplings. Here, we report another example of such an underexplored behavior with three kinked D-B-A systems of $r_{\rm DA} \sim 10$ -19 Å, showing increasing rates of nonradiative charge recombination with increasing r_{DA} . The three D-B-A systems are based on boron dipyrromethene and triphenylamine as electron acceptor and donor groups, respectively, with aryl bridges where the donor and acceptor moieties are connected at *meso*-positions. These D-B-A molecules exhibit radiative electron transfer reactions (or charge-transfer emission), which enables us to experimentally determine the solvent reorganization energy and the electronic couplings. The analysis of charge-transfer emission that explicitly considers electron-vibration coupling, in conjunction with the temperature-dependent analysis and computational method, revealed that the solvent reorganization energy indeed increases with distance and at the same time the electronic coupling decreases with distance expectedly. Therefore, under the right conditions for solvent reorganization energy and electronic coupling values, our results show that we can observe the acceleration of electron transfer reactions with increasing distance even when we have expected distance dependence of electronic coupling. This work indicates that the acceleration of electron transfer with increasing distance may be achieved with a fine tuning of molecular design.

1. Introduction

Electron transfer (ET) is the movement of an electron between donor and acceptor molecules. Despite this simplicity, this reaction remains to be one of mother nature's most important chemical reactions in the production of biologically accessible energy. 1 Multistep ET in photosynthetic reaction center are the fast steps in photosynthesis, resulting in the efficient charge separation and formation of the spin-correlated radical pairs (SCRPs). The detailed studies of the SCRP dynamics, including spin and magnetic field effects on the charge separation and recombination processe,² have revealed the fundamental features of the ET reactions, providing a blueprint for developing small synthetic molecules that mimic photochemical charge separation occurring in these proteins.³⁻⁵ Because of the synthetic accessibility and tunability of their electronic and optical properties, synthetic donor-bridge-acceptor (D-B-A) molecules have also been instrumental for systematic studies of radiation-⁶ and photo-induced⁷ ET events, providing a greater understanding of the parameters that shape ET reaction characteristics, such as electron transfer distances, the Gibbs energy changes, and the spin roles on ET reactions.8 More recently, photogenerated SCRPs are considered as a promising molecular qubit for potential quantum information science (QIS) applications, 9 including quantum computing and communications, ¹⁰ and sensing. ¹¹

Because many ET reactions in the D–B–A molecules systems do not involve the emission of photons, many previous efforts have focused on nonradiative charge separation and recombination reactions. However, photon emission accompanying ET is possible from SCRPs or charge-separated (CS) states. ¹² This type of emission is commonly termed charge-transfer (CT) emission, which arises from the radiative recombination of electrons and holes that are

spatially separated from each other; the general photophysical pathway we consider in this paper is shown in Figure 1a.

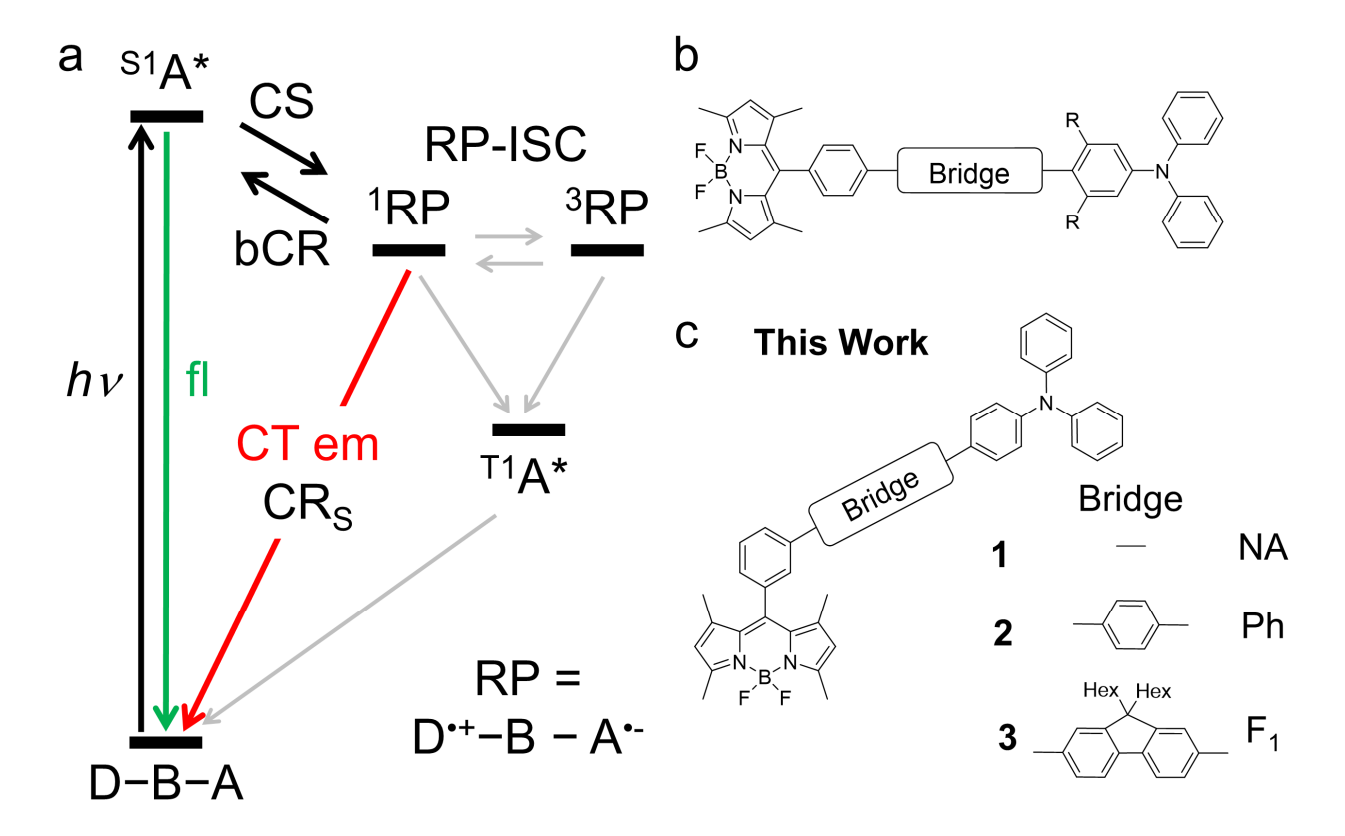


Figure 1. (a) General photophysical pathway with radiative charge recombination from singlet RP. (b) Molecular structures of perpendicular D–B–A molecules studied in refs ¹³ and ¹⁴ where R = H in ref 13 and Me in ref 14. (c) Molecular structures of kinked D–B–A molecules studied in this work.

An important characteristic of CT emission is its sensitivity to the environmental conditions of polarity and polarizability in condensed media. As a result of these properties, CT emission of short-range (donor–acceptor distance, $r_{DA} < 5$ Å) has been utilized in various technologies, such as temperature sensors and responsive biomedical optical imaging probes, ¹⁵⁻¹⁸ as well as organic light emitting diodes, notably as thermally activated delayed fluorescence (TADF) emitters. ¹⁹⁻²⁰ This interesting type of molecular emission has provided the inspiration for our investigations of

the D-B-A molecular systems. While CT emissions from the short-range system are commonly observed and utilized in the applications, reports of CT emission from long-range intramolecular analogs are still scarce. Among the few previously reported are some with donor-acceptor distances remarkably up to $r_{DA} \approx 16$ Å (center-to-center distance) using non-conjugated bridges.²¹⁻²³ As CT emission generally occurs from RPs of singlet character, we could use CT emission as a read out of spin information of SCRPs that act as qubits if one can render singlet RP emissive and at the same time achieve long enough RP state for coherent singlet-triplet mixing to occur; therefore SCRPs can act as optically addressable spin systems. 11 In our previous work, we demonstrated long-range CT emission from D-B-A molecules with r_{DA} up to 24 Å at room temperature, 13 using conjugated bridges that connect boron dipyrromethene (BODIPY or BD) and triphenylamine (TPA) as electron acceptor and donor, respectively. BD also serves as a photon absorber in the visible region. Our molecular design to realize efficient CT emission over long distance is based on intensity borrowing from the oscillator strength of the local excited state.²⁴⁻²⁵ Due to complementary reduction potentials, the combination of BD and TPA provides an appropriate energy gap between (S1BD*) and the RP state (BD*-Bridge-TPA*+) to allow CT emission to occur from typically nonradiative RP states, but their lifetimes are not long (up to ~ 10 ns). 13 An extension of r_{DA} in similar D-B-A molecules based on BODIPY and TPA derivatives was successful in elongating RP lifetime (up to ~ 90 ns at room temperature), ¹⁴ but no CT emission was observed. Yet, with this long RP lifetime, we achieved the magnetic modulation of recombination fluorescence through RP spin dynamics; recombination fluorescence was produced by spin-selective back charge recombination of singlet RPs.¹⁴ The lack of CT emission from this series of molecules may indicate a distance limit of this structural

motif (Figure 1b). Note that we call them perpendicular motifs as the transition dipole moment of the initial excited state (S1BD*) and the direction of ET are perpendicular to each other.

In the current work, we used a kinked bridge group in more compact D-B-A systems with $r_{\rm DA} \approx 10-19$ Å (Figure 1c) to explore their effects on the lifetime of RPs and CT emission. We attempt to manipulate the rates of ET reactions, specifically charge recombination processes, through modulating the magnitude of the electronic coupling between the donor and acceptor by arranging the donor and acceptor moieties at meso-positions, rather than simply extending $r_{\rm DA}$ in the perpendicular motif. Such a kinked bridge group was previously used in other D-B-A molecular systems to promote long-lived RPs.²⁶⁻²⁹ Like our previous series, ¹³ we observed CT emission with decent lifetime from this kinked D-B-A series although the quantum yields of CT emission were smaller than the previous series. Kinetic analysis revealed that unexpected acceleration of nonradiative charge recombination reactions occur at longer r_{DA} while radiative charge recombination rates decrease. This counter-intuitive behavior was predicted by Brunschwig, Ehrenson, and Sutin³⁰ based on the opposing effects of separation distance on electronic couplings (V_{DA}) and the solvent reorganization energy (λ_S): V_{DA} and λ_S are expected to decrease and increase with increasing r_{DA} , respectively. Recently, Kuss-Petermann and Wenger experimentally observed this behavior³¹⁻³² using the D-B-A molecules based on a Ruthenium complex (Ru(bpy)₃), TPA derivatives, and anthraquinone (AQ). Ru(bpy)₃²⁺ acts as a photon absorber/bridge and TPA derivatives and AQ are the electron donor and acceptor, respectively. With this, they observed the increase of charge recombination $(TPA^{\bullet+}-Ru(bpy)_3^{2+}-AQ^{\bullet-}\rightarrow V^{\bullet+})_3^{\bullet+}$ $TPA-Ru(bpv)_3^{2+}-AQ)$ rates with increasing r_{DA} (reaching the max at an intermediate r_{DA}), and qualitatively explained the observation by an increase of the solvent reorganization energy with increasing distance, coupled with a very weak distance dependence (almost distanceindependence) of electronic couplings.³¹⁻³³ Since then, a similar behavior was documented.³⁴ Here, our unique observation of CT emission in a new series of kinked D–B–A molecules enables us to provide further quantitative arguments. We demonstrated a strong dependence of the solvent reorganization energy with increasing distance, while our series of molecules still exhibit an expected distance dependency on electronic couplings. This work indicates that a synthetically small structural modification can shift the balance of reorganization energy and electronic couplings to achieve accelerating electron transfer reactions with increasing distance.

2. Experimental Section

2.1. General Information

All reagents and solvents were sourced from standard commercial chemical supply companies, unless noted otherwise. Silica gel (pore size 60 Å, 230–400 mesh, SiliCycle Inc.) was used in manual, flash column chromatography. The ¹H, and ¹³C NMR spectra were recorded via a Bruker Avance III spectrometer, operating at 400.14 and 100.62 MHz, respectively. The mass spectra were obtained via QStar Elite (AB Sciex) conducted at the Laboratory of Mass Spectrometry and Omics Analysis of the University of Connecticut Department of Chemistry. UV-vis absorption spectra were recorded by a Cary 50 Scan UV-vis spectrophotometer (Varian). A FLS1000 photoluminescence spectrometer (Edinburgh Instruments) was used to record the steady-state and time-resolved emission. Fluorescence lifetime measurements were performed using a TCSPC system of the FLS1000 equipped with a TCSPC/MCS/counter module (TCC2), a Hamamatsu H10720-01P, and a pulsed diode laser (EPL-510) as the excitation source that provided 506 nm excitation having a pulse duration 85 ps. Using the FLS1000 equipped with an integrating sphere, absolute measurements were conducted to obtain quantum yields of fluorescence (Φn). Quantum yield of CT emission (ΦcT) were determined by referencing to Φn of

the same molecules. Unless explicitly mentioned, all the photophysical characterization was conducted at room temperature (20 °C).

2.2. Synthesis

The synthetic scheme, detailed procedures, and characterizations of three BD-Bridge-TPA molecular systems are described in Supporting Information.

2.3. Nanosecond Transient Absorption Spectroscopy (ns-TA)

A ns-TA system was created based around the LP920 laser flash photolysis / transient absorption spectrometer (Edinburgh Instruments). This instrument was coupled with a third harmonic (355 nm) of Nd:YAG as the pump (Continuum Surelite I, pulse width fwhm 5-7 ns, 10 Hz rep. rate), a X Model 920 450 W xenon arc lamp for a probe lamp, and a monochromator. The monochromator is coupled with an iCCD camera (Andor Technology) to conduct spectral measurements, and a P928 photomultiplier detector (Hamamatsu) to conduct kinetic measurements. The pump beam was operated at an energy range of 2-7 mJ, depending on the measurements conducted, with minor fluctuations that were accounted for. Samples were prepared in 1.0 cm optical glass cuvettes for measurements. Triplet quantum yields (Φ_T) were calculated via a relative actinometry method with benzophenone in acetonitrile (MeCN) as a reference ($\Phi_T = 1.0$).³⁵ The ns-TA system was also fitted with a 3470 electromagnet (GMW), powered by the Bipolar Power Operational Power Supply/Amplifier (Kepco), for magnetic field measurements. The details of this setup were reported elsewhere.³⁶ Datasets were processed and analyzed using OriginPro 2017.

2.4. Femtosecond Transient Absorption Spectroscopy (fs-TA)

A fs-TA system was used based on the HELIOS FIRE (Ultrafast Systems), coupled with a femtosecond laser system (Coherent). The details were reported elsewhere.³⁶ Datasets obtained

were processed and analyzed with the software Surface Xplorer (Ultrafast Systems) via fluorescence background subtractions, applied chirp correction, time-zero adjustments, single value decomposition, global fitting, and kinetic fitting.

2.5. Electrochemistry

Cyclic voltammetry measurements were conducted on all three samples based around a 600E Electrochemical Analyzer/Workstation (CH Instruments). This system was equipped with a standard three-electrode cell comprised of a pseudo-Ag reference electrode, a Pt wire counter electrode, and a 3 mm glassy carbon-disk working electrode in an acetonitrile (MeCN) solution of 0.1 M tetrabutylammonium hexafluorophosphate (TBA⁺PF6⁻). Datasets were processed and analyzed with software CHI600e (CH Instruments). Potentials measured are referenced vs Fc^{+/0}; ferrocene was introduced before measurements were conducted. Spectroelectrochemical measurements were performed with a honeycomb spectroelectrochemical cell (PINE research) coupled to the 600E Electrochemical Analyzer/Workstation. Samples were prepared in MeCN with 0.1 M TBA⁺PF6⁻.

2.6. Computations

Computations were carried out with Gaussian16.³⁷ The geometries were optimized with B3LYP functional³⁸⁻³⁹ in density functional theory (DFT) calculations. The geometry optimizations were performed without symmetry constraints. Calculations on radical anions and cations were spin-unrestricted. The 6-31G+(d) for the ground states and 6-31G(d) for the excited states basis set were used for the geometry optimization and all other single-point calculations. TDDFT single-point energy calculations were performed with B3LYP, PBEPBE,⁴⁰⁻⁴¹ CAM-B3LYP,⁴² and ωB97XD.⁴³ The polarizable continuum model (PCM) for solvation in chloroform was used as implemented in Gaussian.⁴⁴⁻⁴⁶

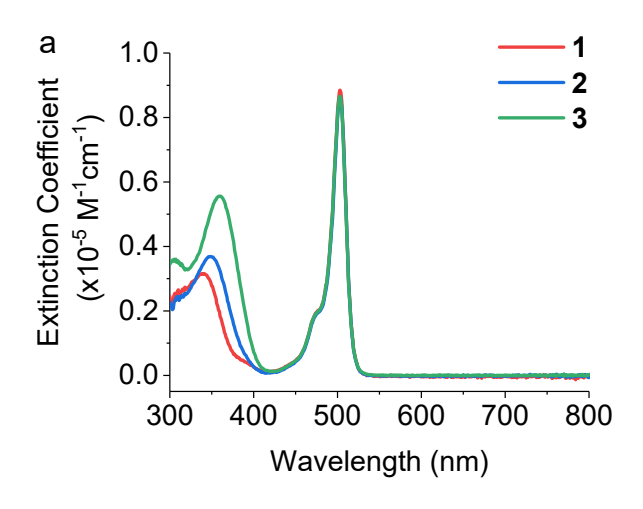
3. Results

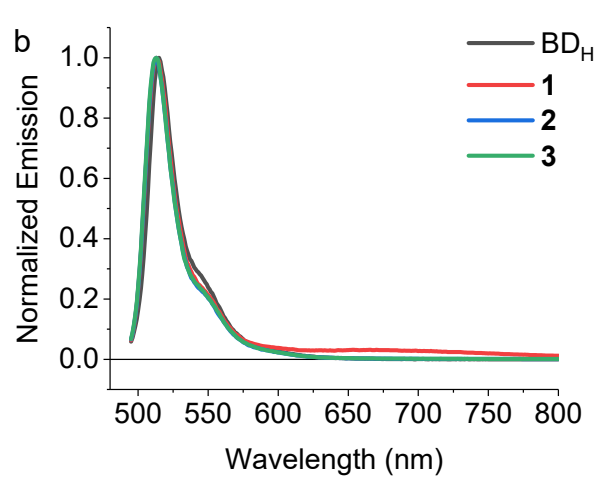
3.1. Synthesis

Three kinked BD–Bridge–TPA molecular systems where Bridge is no additional bridge (NA), phenyl (Ph), and fluorene (F₁), were successfully synthesized (Figure 1c). We used a one-pot two-step Suzuki coupling for Ph and F₁ bridges, which helps avoid the isolation of the aryl boronic esters.⁴⁷

3.2. Observation of CT emission

We recorded the steady-state absorption and emission spectra in chloroform, in which we observed CT emission in the previous series. ¹³ The absorption spectra are shown in Figure 2a, with little change for the absorption band of BD moieties across the series, all similar extinction coefficients values ($\varepsilon \approx 8.6 \text{ x } 10^4 \text{ M}^{-1} \text{ cm}^{-1}$), like previously reported BD-Bridge-TPA molecules ¹³⁻¹⁴ and other similar BDs. ⁴⁸⁻⁵⁰ The absorption and emission spectra of the parent BD are shown in the Supporting Information (Figure S1). The r_{DA} are reported in Table 1. They were determined computationally based on center-to-center distances from DFT optimized geometries. We also estimated r_{DA} based on an electron-hole separation of the RP state identified in TDDFT calculations, ⁵¹⁻⁵² which is ~1 Å shorter than the structural estimates (Table 1).





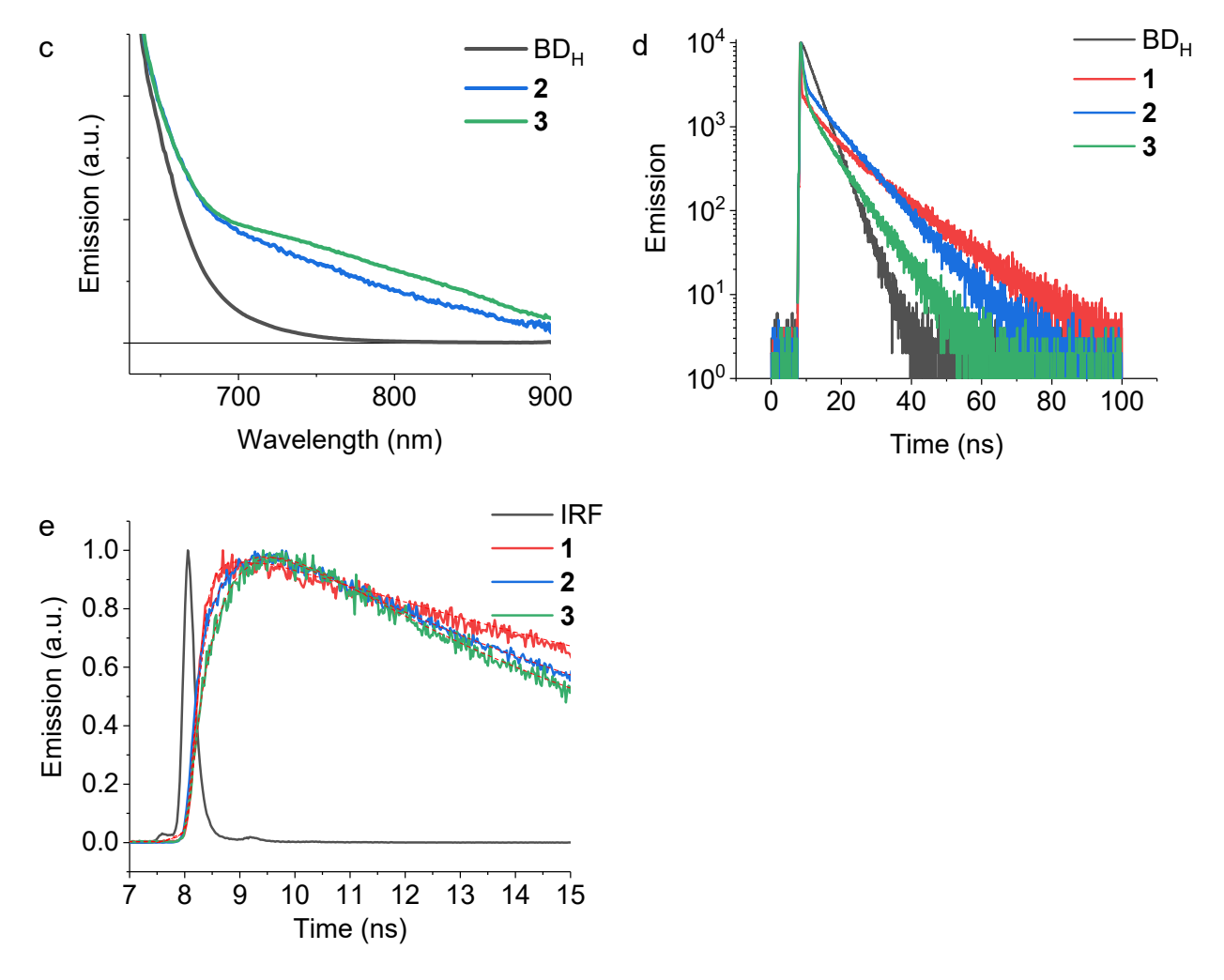


Figure 2. CT emission recorded from the D–B–A compounds dissolved in chloroform. (a) Absorption spectra of 1-3 and BD ($\lambda_{max}\approx 501$ nm). The absorption bands in the 300–400 nm region in longer bridges can be correlated to the bridge moiety. (b) Emission spectra of 1-3 and BD ($\lambda_{ex}=470$ nm). For clarity, the spectra are normalized to the emission maxima ($\lambda_{max}\approx 512$ nm) of BD fluorescence. The fluorescence emission in the normalized emission spectrum region 600-800 nm is attributed to the CT emission. (c) Zoom-in figure comparing the emission spectrum of 2 and 3 and BD shows CT emission more clearly. (d) Decay profiles of BD emission ($\lambda_{em}=520$ nm) and (e) CT emission ($\lambda_{em}=760$ nm) of 1, 2, and 3 in chloroform ($\lambda_{ex}=506$ nm). The redlines are fits to the biexponential decays. IRF = instrument response function.

Table 1. Photophysical Properties of D-B-A Series^a

| Compounds | Bridge | <i>r</i> да (Å) ^b | $\Delta G_{\mathrm{CS}}^{\circ}$ (eV) ^c | E _{RP} (eV) ^c | $\Phi_{\mathrm{fl}}{}^{\mathrm{d,e}}$ | $\Phi_{\mathrm{CT}}^{\mathrm{e,f}}$ | $\Phi_{	extsf{T}}^{e,g}$ |
|-----------|----------------|---------------------------------|----------------------------------------------------|-----------------------------------|---------------------------------------|-------------------------------------|--------------------------|
| 1 | NA | 10.1 (9.2) | -0.097 | 2.35 | 0.084 | 0.017 | 0.6 |
| 2 | Ph | 14.3 (13.1) | -0.025 | 2.43 | 0.35 | 0.013 | 0.3 |
| 3 | F ₁ | 18.6 (16.7) | -0.037 | 2.41 | 0.23 | 0.003 | 0.06 |

^aReported in chloroform at 20 °C. ^bDonor–acceptor distance, determined as the center-to-center length from DFT optimized structures. The values in the parentheses are determined as the electron-hole separation of the RP state TDDFT calculations. ^cEstimated from exponential fittings of biphasic fluorescence lifetime decays. The energy of ^{S1}BD* is determined from the intersection of the absorption and emission spectra for 1-3. ^dQuantum yield of fluorescence. Determined by the absolute method. ^eErrors are typically $\pm 10\%$. ^fQuantum yield of CT emission, determined by referencing to Φ_{fl} of the same molecule. ^gQuantum yield of the triplet excited state of BD (^{T1}BD*).

Upon photoexciting the BD acceptor moiety ($\lambda_{ex} = 470$ nm) in the molecular systems 1 – 3, we observed fluorescence ($\lambda_{max} \approx 512$ nm) from the BD along with a broad emission band spanning the region from 600–1000 nm (Figure 2b). We assigned this broad emission as CT emission from RP to the ground state (GS); BD*-Bridge-TPA*+ \rightarrow BD-Bridge-TPA. This emission is not correlated to aggregation of exciton emission, due to samples being prepared and measure at concentrations < ~1-5 μ M, and no significant concentration dependence was observed. The quantum yields of emission are reported in Table 1, showing the trend of decreasing Φ_{CT} decreasing with increasing r_{DA} . Φ_{CT} are generally smaller than those of the perpendicular motif at a comparable distance.¹³ Note that the normalized emission spectra in Figure 2a make Φ_{CT} appear much smaller in 2 and 3 compared to 1 because of larger Φ_{Π} in 2 and

3. Yet, molecular system 3 of the longest r_{DA} still has measurable CT emission; a zoomed-in emission spectra for 2 and 3 is shown in Figure 2c, illustrating the presence of CT emission more clearly.

Time-resolved emission measurements showed biphasic decays of the BD fluorescence for 1 – 3 in chloroform (Figure 2d), with the faster component (k_{fast}) being an order of magnitude, or more, faster than the fluorescence lifetime of BD alone (Supporting Information, Table S1). This difference suggests that a major deactivation route exists, the CS pathway. The slower component (k_{slow}) of the biphasic decay was also an order of magnitude, or more, slower than k_{fast} , which can be attributed due to recombination fluorescence of $^{S1}BD^*$, following back charge recombination from the singlet RP state (bCR). Fitting the biphasic fluorescence lifetimes, as previously described, $^{53-54}$ we determined ΔG_{CS}° in chloroform (Table 1), along with k_{CS} , k_{bCR} and total k_{CR} (Supporting Information, Table S1). In a similar manner to the previous series, $^{13-14}$ due to the proximity in energy of the $^{S1}BD^*$ and RP states ($\Delta G_{CS}^{\circ} \sim -30-100$ meV), within the thermal equilibrium range, efficient charge recombination to the initial excited state and the resulting recombination fluorescence is realized. Time-resolved emission measurements of CT emission clearly showed the rise, slower than the instrument response function (IRF) of our instrument (Figure 2e).

To gain further insights into the nature of CT emission and kinetics, we performed temperature-dependent steady-state emission measurements as well as lifetime measurements (both on BD fluorescence and CT emission) in the range of 5 - 60 °C. Expectedly, the CT emissions are temperature dependent, and they almost disappear at higher temperatures, favoring the back charge recombination and reproduction of $^{S1}BD^*$ (Supporting Information, Figure S2).

3.3. Unexpected Acceleration of Nonradiative Charge Recombination

In addition to the evidence for CT emission provided by the biphasic decays of BD fluorescence, the femtosecond transient absorption measurements provide supporting evidence that RP state formation is occurring. The spectra and kinetics of 1 in chloroform are shown in Figure 3 and the spectra of 2 and 3 are shown in Supporting Information Figure S3.

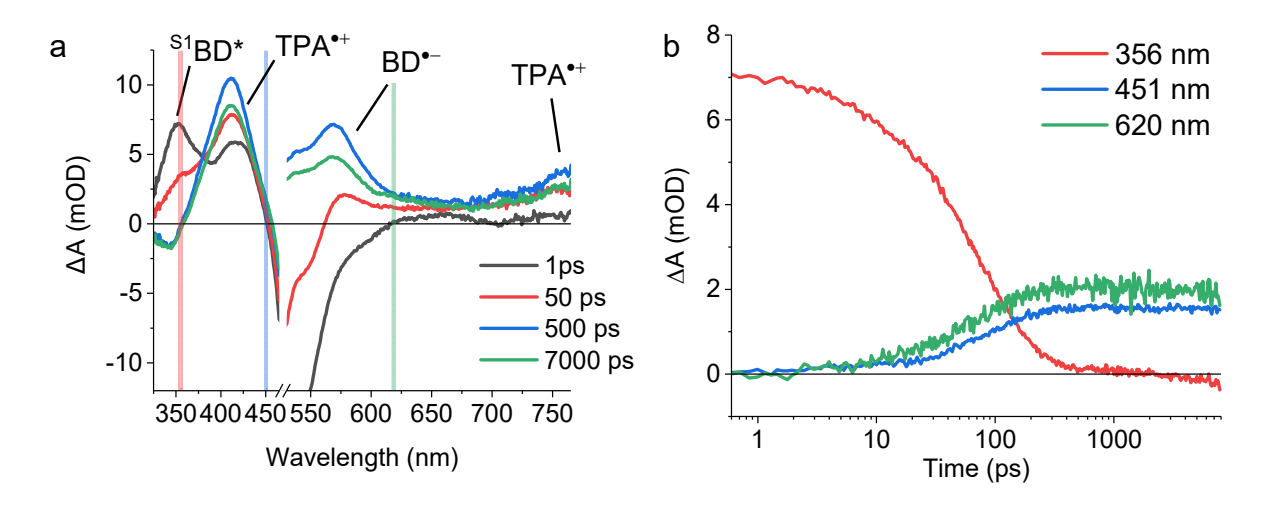


Figure 3. Identification of radical pair formations upon photoexcitation of BD. (a) Transient absorption spectra of **1** at 1, 50, 500, 7000 ps after the fs laser pulse (λ ex = 500 nm) in chloroform. (b) Decay kinetics of **1** monitored at respective wavelengths at 356, 451, and 620 nm roughly correspond to the isosbestic points for ^{S1}BD*, TPA* and BD* (color coded in panel a).

We assigned the transient absorption bands using the previously reported spectral signature of the BD radical anion (BD $^{\bullet}$, at ~ 560 - 570 nm),³⁶ and with the absorption spectra of the electrochemically produced radical cation BD–Bridge–TPA $^{\bullet}$ (Supporting Information, Figure S4). While the spectra of radical cations shift depending on the bridge lengths, reduction potentials of BD and TPA radical cation are relatively independent of the bridge lengths, arguing that charges are expected to be largely localized in each moiety (Table S2). At the same time,

less positive reduction potentials of TPA radical cation with longer bridges (~20-40 meV) of the current series may indicate a slight delocalization on to the bridge. DFT calculations show that the angles between the longest axis of BODIPY (which corresponds to the transition dipole moment of S1BD*50) and the line connecting the center-to-center of the charged species (direction of ET reactions) stay relatively constant; 38°, 44°, 41° for 1, 2, 3, respectively (Supporting Information, Figure S5). With this series of data, we, therefore, use center-to-center distance as a measure of charge separation (rDA in Table 1). No transient absorption bands were seen corresponding to a reduced or oxidized bridge moieties, indicating that the bridge moieties are likely not involved directly in the ET process, instead acting as a virtual state for tunneling. This is expected, due to the very unfavorable driving forces for ET reactions to either oxidize or reduce the bridge moieties (Ph and F₁) based on their reduction and oxidation potentials.⁵⁵⁻⁵⁸ Specifically, the oxidation potential of Ph and F_1 are reported as $\sim 2.1^{58}$ and 1.3 V vs $Fc^{+/0}$, respectively,⁵⁷ which are significantly higher than that of BD (~0.8 V vs Fc^{+/0}) and TPA (~0.5 V vs Fc^{+/0}). Please see Supporting Information, Table S2 for the values in the current series of D-B-A. Therefore, this set of data supports the tunneling mechanism of the ET reactions. The rate constants (k_{CS} and total k_{CR}), estimated from the global fitting are reported in Table 2. Importantly, the measured k_{CS} (either by global fitting or fitting at single wavelengths at the isosbestic points where appropriate) are comparable to the CT emission rise time (Table 2) as well as the rate constants obtained from the fitting of biphasic decay of BD fluorescence lifetime (Supporting Information, Table S1). Combined, our data clearly supports that the longwavelength emissions are indeed CT emission (radiative charge recombination).

Table 2. Nonradiative and Radiative Electron Transfer Rates^a

| | | $k_{\rm S1}$ | kcs | | | $k_{\rm CR}$ (tot) | $k_{\rm CRS}$ | $k_{ m rad}$ |
|-----------|----------------|----------------------------|-----------------------------|----------------------------|---------------------------|------------------------|---------------------------|------------------------|
| | | (s ⁻¹) | | (s ⁻¹) | | (s ⁻¹) | (s^{-1}) | (s ⁻¹) |
| Compounds | Bridge | fsTA global | fsTA global ^b | fsTA rise ^c | CT em rise ^d | fsTA global | e | f |
| 1 | NA | 1.38 × 10 ¹⁰ | 1.35 × 10 ¹⁰ | 1.01 × 10 ¹⁰ | 6.94 × 10 ⁹ | 3.35×10^{7} | 2.63 × 10 ⁷ | 1.15 × 10 ⁶ |
| 2 | Ph | 2.79 × 10 ⁹ | 2.52 × 10 ⁹ | 2.60 × 10 ⁹ | 2.46 × 10 ⁹ | 6.83 × 10 ⁷ | 6.96 × 10 ⁷ | 1.33 × 10 ⁶ |
| 3 | F ₁ | 2.45 × 10 ⁹ | 2.18 × 10 ⁹ | 2.13 × 10 ⁹ | 1.98 × 10 ⁹ | 9.53 × 10 ⁷ | 1.19 × 10 ⁸ | 3.66 × 10 ⁵ |

^aReported in chloroform at 20 °C. ^bEstimated by $k_{\rm CS} = k_{\rm S1}({\rm D-B-A}) - k_{\rm S1}({\rm BD})$ where $k_{\rm S1}({\rm BD}) = 2.7 \times 10^8$ (s⁻¹) determined by the fluorescence decay of BD alone. ^cDetermined by the rise time of radical anions or cation peak (isosbestic point). ^dDetermined by the rise time of CT emission kinetics measured by the TCSPC method: $k_{\rm CS} \sim k_{\rm rise}$. ^e $k_{\rm CRS} = (k_{\rm CR}({\rm tot}) - k_{\rm rad}) \times (1 - \Phi_{\rm T})$ where we used $k_{\rm CR}$ (tot) measured by the CT emission decay. ^f $k_{\rm rad} = k_{\rm CR}$ (tot) × Φ_{CT}/φ_{CS}.

The initial charge separation occurs with $\phi_{CS} \ge 92\%$ for 1-3, which is expected from fluorescence decay being an order of magnitude faster than that of BD alone and the rapid appearance of the RP states seen in the TA spectra (Figure 3). We determined ϕ_{CS} under equilibrium condition using a similar approach employed for TADF.⁵⁹ Using π -conjugated bridges enables this efficient charge separation, even without large driving forces at play and with the kinked bridges. Thus, the relatively low Φ_{CT} reported for 1-3 in chloroform is not a result of inefficient initial charge separation, rather likely a result of the charge recombination pathways branching from the RP states (Figure 1).

Following the confirmation of RP state formation, TA measurements were conducted on a ns timescale to better examine if the RP states being generated in 1-3 had sufficiently long lifetimes

for coherent singlet-triplet mixing, allowing potential magnetic field effects to be explored.⁶⁰ We determined that the lifetimes of the RPs were at most 10-20 ns long, in agreement with the lifetime of recombination fluorescence (k_{slow}). These lifetimes are likely insufficient durations for coherent singlet-triplet mixing to occur, and we did not observe any measurable magnetic field effects on the radicals and triplet excited states at the field strengths of 0 to 600 millitesla.

We also determined the quantum yields of the triplet excited state (Φ_T) of the local BD state (T1BD*) (Table 1). We used $\lambda_{ex} = 355$ nm as the excitation source in nsTA because of the instrument's limitation. In the same way as previously, 14, 36 we confirmed that the excitation in this region results in the ultrafast energy transfer from the excited states of TPA/Bridge to S1BD* (<1 ps), followed by the almost identical photophysical pathways as the case with photoexcitation at the BD core (Supporting Information, Figure S6). We then used Φ_T to determine the rates of nonradiative charge recombination of singlet RP, kcrs (Table 2). Here, we assumed that the singlet RP state can either recombine spin selectively to form the GS or can form T1BD*. We did not attempt to discriminate between the two possible pathways of the formation of ${}^{T1}BD*$ (${}^{1}RP \rightarrow {}^{3}RP \rightarrow {}^{T1}BD*$ or ${}^{1}RP \rightarrow {}^{T1}BD*$), though the former is more likely the case. With ϕ_{CS} , Φ_{CT} , and k_{CR} in hand, we also determined the radiative rate constants of CT emission ($k_{\rm rad}$) and nonradiative charge recombination of singlet RP ($k_{\rm CRS}$). We observed a decrease in $k_{\rm rad}$ with increasing $r_{\rm DA}$ (Table 2), but unexpectedly observed an increase in $k_{\rm CRS}$ with increasing r_{DA} (Figure 4). In the following discussion, we focus on this counter-intuitive result of increasing nonradiative singlet charge recombination rates at longer distances. While we aid the analysis with the information obtained from the CT emissions, we do not provide a thorough analysis of CT emission, which will be described in future studies.

We would like to note that our discussion centers on the effects of solvent reorganization and electronic couplings. In the prior work by Kuss-Petermann and Wenger,³¹⁻³³ two other possible effects were deemed negligible and not explicitly considered: they are spin effects (i.e., singlet vs triplet charge recombination of RPs)⁶⁰⁻⁶¹ and electron-vibration (e-v) coupling effects (especially in the Marcus inverted region),⁶²⁻⁶³ both of which could result in accelerating charge recombination. While we determined spin-selective charge recombination rates to exclude the spin effect, the nature of our current analysis did not completely exclude the possible effects of e-v coupling.

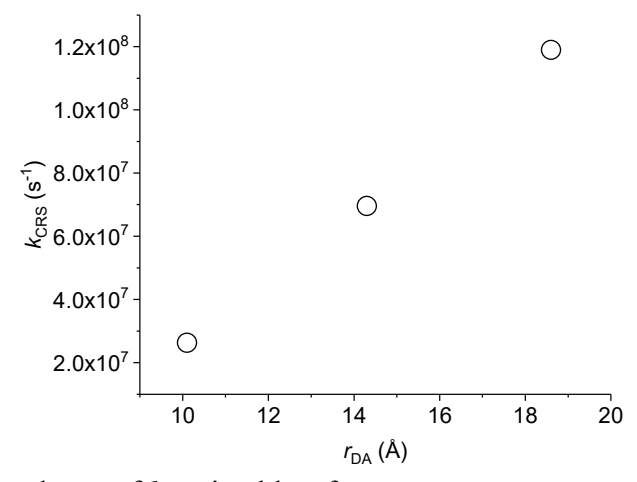


Figure 4. Distance-dependence of k_{CRS} in chloroform.

4. Discussion

4.1. Semiclassical Marcus Equation

We observed the trend of increasing k_{CRS} with increasing r_{DA} for 1-3. As the electronic coupling V_{DA} usually decreases with increasing r_{DA} , we would expect to see a decrease in ET rates if all other terms are held fixed, based on the "high-temperature limit" of the semiclassical Marcus equation:

$$k_{ET} = \frac{2\pi}{\hbar} |V_{DA}|^2 \frac{1}{\sqrt{4\pi\lambda k_B T}} exp\left(-\frac{(\Delta G^{\circ} + \lambda)^2}{4\lambda k_B T}\right)$$
 (1)

where V_{DA} is the electronic coupling between the initial and final states of ET reactions, and \hbar , k_{B} , and T are the reduced Planck constant, the Boltzmann constant, and Temperature, respectively. Here, λ is the total reorganization energy (λ_{tot}). The Marucs theory does predict a regime exists such that ET rates will continue to increase until hitting a maximum at an optimal r_{DA} , with further increases in r_{DA} resulting in decreases of ET rates.³⁰ The key to this is a reorganization energy λ that can outweigh the effect of V_{DA} resulting in faster ET rates as r_{DA} increases. Despite this prediction, this has remained a largely unconsidered effect in the studies of ET reactions, except for a few cases.⁶⁴⁻⁶⁵ Kuss-Petermann and Wenger demonstrated this trend experimentally with their D–B–A constructs³¹⁻³² where they observed almost distance-independent V_{DA} while λ increased with increasing r_{DA} , providing a qualitative argument for the reasoning behind this counter-intuitive behavior.

Reorganization energy λ_{tot} is the sum of solvent and internal reorganization (λv) energies: $\lambda_{tot} = \lambda_S + \lambda v$. Usually, λv 's are assumed to be relatively constants in homologous D–B–A series when charge delocalization does not change across the series. In our rigid D–B–A systems, with 1-3 only differing by their bridge group, we expect that there is a small difference in λv across within series; little distance dependence. Electrochemical measurements support this to some extent as mentioned above.

In contrast to λv , λs , the energy for the reorganization of the solvent molecules solvating the D–B–A system during ET reaction, can have a large distance dependence. A simple dielectric continuum model of λs , or the Marcus two-sphere approach, ⁶⁶ is

$$\lambda_{\rm S} = \frac{e^2}{4\pi\varepsilon_0} \left[\left(\frac{1}{2r_{\rm D}} + \frac{1}{2r_{\rm A}} - \frac{1}{r_{\rm DA}} \right) \left(\frac{1}{n^2} - \frac{1}{\varepsilon_{\rm r}} \right) \right] \tag{2}$$

where ε_0 is the vacuum permittivity constant, r_D and r_A are the donor and acceptor radii, n and ε_r are the refraction index and the static dielectric constant for the solvent, respectively.

Generally, determination of reorganization energies is one challenging task in the field of ET reactions. Figure 3. Internal reorganization energies may be estimated by resonance Raman studies, for but their applications can be limited. The case in point of this work is solvent reorganization energy. The dielectric continuum model of λ s (eq. 2) is widely used as an estimate of λ s and it does predict a larger value at increasing r_{DA} , but it is noted that eq. 2 underestimates the distance dependence as it does not incorporate molecular details, and it also has other shortcomings. Alternatively, one can use a molecular modeling approach that takes into account the discrete nature of solvent molecules and the solute. Experimentally, one may use temperature-dependence of ET reactions or the Arrhenius analysis (AA). Kuss-Petermann and Wenger used AA with eq. 1 to obtain λ_{tot} (they considered λ_V negligible and used λ_{tot} as λ s), assuming λ_{tot} and V_{DA} are temperature independent. Under the same assumption, we also performed the analysis on k_{CRS} . The Arrhenius plots ($\ln\left(k_{CRS}T^{\frac{1}{2}}\right)$ vs 1/T) is shown in Supporting Information, Figure S7. While we also observed the decrease in λ_{tot} with increasing r_{DA} (Table 3), the λ_{tot} values turn out to be too large and not consistent with the other aspects of ET reactions (see Section 4.2).

Table 3. Solvent Reorganization Energies and Electronic Couplings in Chloroform

| | | λ_{tot} | λs | | λv | | $V_{ m DA}$ | | | | |
|-----------|--------|--------------------------|-------------------|-----------------------------|-------------------|------------------------------------|----------------------------------|------------------|------------------|--------------------|--|
| | | (eV) | (eV) | | (eV) | | (cm ⁻¹) ^a | | | | |
| Compounds | Bridge | AAb | spec ^c | two- sphere ^d | spec ^c | AA /two- sphere ^e | AA | rad ^f | GMH ^g | eq. 4 ^h | |
| 1 | NA | 1.27 | 0.47 | 0.57 | 0.16 | 0.75 | 28 | 190 | 240 (190) | 880 | |
| 2 | Ph | 1.42 | 0.54 | 0.68 | 0.23 | 0.73 | 17 | 155 | 150 (200) | 300 | |

| 3 | \mathbf{F}_1 | 1.73 | 0.60 | 0.74 | 0.23 | 0.99 | 3 | 65 | 120 (130) | 200 |
|---|----------------|------|------|------|------|------|---|----|-----------|-----|
| | | | | | | | | | (130) | |

^a V_{DA} of the ¹CS and GS states. ^b Determined by the Arrhenius analysis (AA). ^c Determined by the fittings of CT emission. ^d Determined by the two-sphere model (eq. 2). ^e Reported values are determined by $\lambda v = \lambda_{tot}$ (AA) – λ_{S} (two-sphere model). ^f Determined by eq. 6. ^g Determined by eq. 7. The values in the parentheses are the coupling values at the geometry of the RP state. ^h Determined by eq 4. with λ 's determined by the fitting of CT emission.

There are also reports that indicate λ_S decrease with increasing r_{DA} . Therefore, to add to the qualitative argument of Kuss-Petermann and Wenger's work, our work here sought to determine the value of λ_S experimentally with CT emission measurements. In the next section, we described our analysis.

4.2. Spectral Analysis of CT Emission

Radiative charge recombination or CT emission coupled the same initial (1 RP) and final (GS) states as nonradiative charge recombination, therefore there is a close relationship between thermal electron transfer and radiative CT reactions. $^{73-76}$ Marcus 75 showed that simultaneous analysis of CT absorption and emission spectra yield an accurate determination of the ET parameters, such as the Gibbs energy, magnitude of electronic coupling V_{DA} , and reorganization energies λ . We could obtain the estimates from either one of them. Taking advantage of these unique features, some earlier works, including the work on intermolecular D/A systems by Gould and Farid, $^{77-78}$ the work on intramolecular (solvent-coupled) D–B–A molecules by Zimmt and Waldeck, 54 , $^{79-80}$ and by Heitele and Jortner 81 extensively utilized CT absorption and emission spectra to quantify the ET parameters.

The intensity of emission I(v) is given by

$$I(v) \propto v^3 |M(v)|^2 FC(v)$$
 (3a)

where M(v) is the transition moment at frequency v and FC(v) is the Franck-Condon factor. While the intensity borrowing and therefore the electronic coupling between the singlet excited state and the RP (V^*) , in addition to V, can be substantial in determining M(v), it is difficult to establish the exact contributions in the current case. Here, we only consider the band shape, and therefore we have chosen to describe the reduced intensity in terms of $FC(v) = I(v)/v^3$ in a similar manner to the earlier work^{77,81}

$$\frac{I(v)}{v^3} = \sum_{w=0}^{\infty} \left(e^{-S_{\rm HR}} \frac{S_{\rm HR}^w}{w!}\right) \exp\left[-\frac{\left(\lambda_{\rm S} + \Delta G^0 + w\hbar\omega + hv\right)^2}{4\lambda_{\rm S}k_{\rm B}T}\right]$$
(3b)

where $S_{\rm HR} = \frac{\lambda_{\rm V}}{\hbar\omega}$ is the Huang-Rhys factor characterizing the strength of e-v coupling, and ω is only one high frequency of the coupled quantum mechanical vibration modes. This is formally similar to the expression for a semiclassical Marcus equation that considers high-frequency (>> $k_{\rm B}T/h$) vibrations of electron donor and acceptor molecules (e-v coupling), represented by a single ("average") quantized mode, ⁸²⁻⁸⁴

$$k_{\rm ET} = \frac{2\pi}{\hbar} |V_{ab}|^2 \frac{1}{\sqrt{4\pi\lambda_{\rm S}k_{\rm B}T}} \sum_{w=0}^{\infty} (e^{-S_{\rm HR}} \frac{S_{\rm HR}^w}{w!}) \exp\left[-\frac{(\lambda_{\rm S} + \Delta G^0 + w\hbar\omega)^2}{4\lambda_{\rm S}k_{\rm B}T}\right]$$
(4)

Accurate characterization of all the parameters is difficult in the absence of structure in CT spectra. Experimentally, we measured ΔG^0 from the emission lifetime experiments (Table 1). The rest of the parameters (λ s, λ v, and $\hbar\omega$) are variable. We fixed the e-v coupling $\hbar\omega$ based on the DFT calculations ($\hbar\omega = 0.171 \text{ eV} \sim 1370 \text{ cm}^{-1}$); we used the average frequency that is obtained as a sum of all the frequencies that are typically characteristics to C=C modes⁸⁵ weighted with their relative intensities of the GS-optimized structures, in a similar manner to the work by Matyushov.⁸⁶ All three molecules have similar average frequencies. Representative fittings of CT emission spectra are shown in Figure 5 and the fitted values are reported in Table 3.

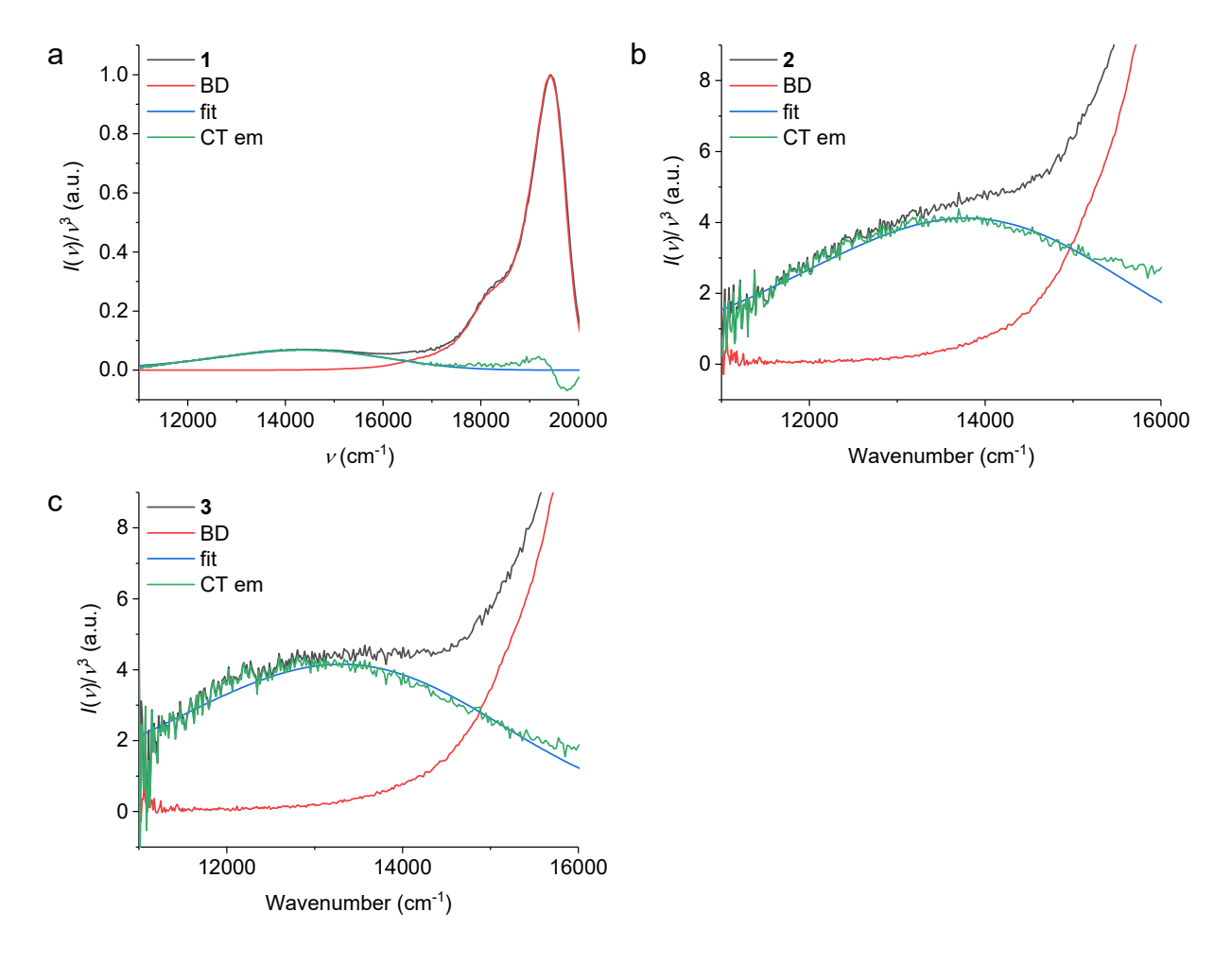


Figure 5. Spectra fits of CT emission with eq. 3b; (a) **1**, (b) **2**, (c) **3** in chloroform at 20 °C. Red lines are BD fluorescence emission. CT emissions lines were determined by subtracting the BD emission from the emission spectra.

We could obtain reasonable fits with other combinations of λ and $\hbar\omega$. For example, DFT calculations provide $\lambda_V = 0.14$ eV (based on the individual donor and acceptor moieties), and we can use this value as a fixed λ_V to fit the spectra to obtain $\lambda_S = 0.48$, 0.62, and 0.69 eV for 1, 2, 3, respectively. It is interesting to note that λ_V by the DFT calculation is fortuitously close to that obtained for 1 by the fitting without constraints. On the other hand, larger λ_V values for 2 and 3 estimated by the fittings might point to a slight delocalization of charges (likely positive charges on TPA) as suggested by the electrochemical measurements (Supporting Information, Table S2).

However, not all the combinations would work. Notably, we could not fit the CT emission spectra with λ_{tot} estimated from the Arrhenius plots and the Marcus two-sphere model for λ_{S} (Table 3). This failure can be easily seen by inspecting the peak of CT emission that is approximately characterized by⁷⁵

$$h\nu_{\text{max}} \simeq -(\Delta G_{\text{CR}} + \lambda_{\text{S}} + \lambda_{\text{V}} + \hbar\omega)$$
 (5)

If we use λ_{tot} from the AA (and neglecting the specific vibrational mode contribution) the experimentally obtained ΔG_{CR} (= E_{RP} , Table 1), we obtain hv_{max} = 1.08, 1.01, and 0.68 eV. They are significantly lower than actual values of hv_{max} that are 1.77, 1.70, 1.65 eV for 1, 2, and 3, respectively (Figure 5). This showed the limitation of using eq. 1 which is without electron-vibration couplings, at least in our case. We could also not fit the spectra well without incorporating high-frequency (>> $k_{\text{B}}T/h$) vibrational mode, highlighting its importance.

The spectral analysis supports the trend that λ_S increases with increasing r_{DA} while the values by the spectral analysis are smaller than the Marcus two-sphere model. More detailed analysis of CT emission spectra, including their temperature-dependent behaviors and possible effects on λ , are underway.

4.3. Distance Dependence of Electronic Couplings

We now examine the distance dependence of electronic couplings, V_{DA} , for 1-3, to see if V_{DA} is almost independent of the distance. While the Arrhenius analysis (AA) with eq. 1 resulted in a reasonably small and distance dependent V_{DA} values, we decided to use other methods to independently estimate V_{DA} because the AA yields too large λ_{tot} values to account for the CT emission data (see Section 4.2). Here, we employed a couple of other methods, including use of radiative decay rate within a two-state model and the generalized Mulliken-Hush (GMH) analysis.

We determined V_{DA} using the radiative decay constant (k_{rad}) within a two-state model (RP and GS) with only V_{DA} ;^{24,87}

$$k_{\rm rad} = \frac{32\pi^3 n^3}{3\hbar} |V_{\rm DA} \Delta \mu|^2 \langle v \rangle \tag{6}$$

where $\Delta\mu$ is the change in dipole moment accompanying electron transfer and $\langle v \rangle$ is the first moment of the emission band, which is taken as the peak energy of the CT emission band. As seen, the radiative decay method does not require the information of λ s. While we expect that a three-state model that includes the local excited state^{25, 88-89} would be well-suited like in our previous case,¹³ we did not use a three-state model partly because of the lack of measurable CT emission in enough number of solvents at the moment. Nonetheless, judging from the values, a two-state model appears to yield reasonable $V_{\rm DA}$ values (Table 3). The obtained values have exponential distance with the attenuating factor $\beta \sim 0.13 \pm 0.01$ Å⁻¹ (Supporting Information, Figure S8). Compared with the reported coupling values determined with the same two-state model, the current coupling values are expectedly larger than those for non-conjugated bridges,²² but a couple of times smaller than contact ion pairs/exciplex^{77, 90} and slightly smaller than a porphyrin-[60]fullerene conjugate (assumed at contact distance ~ 4 Å).⁹¹

We also applied the two-state GMH analysis to compute $V_{\rm DA}$. The applications of GMH to photoinduced electron transfer reactions are well documented, $^{92-93}$ and we also employed it before. Extending the Mulliken-Hush approach, 74 , 87 Newton and Cave $^{94-95}$ expressed $V_{\rm DA}$ (or $V_{\rm ab}$ in the equation below) in terms of the experimentally accessible adiabatic parameters as

$$V_{\rm DA} = V_{\rm ab} = \frac{\mu_{12}\Delta E}{\Delta \mu_{\rm ab}} = \frac{\mu_{12}\Delta E}{((\Delta \mu_{12})^2 + 4(\mu_{12})^2)^{1/2}}$$
(7)

where a and b represent initial and final states of the system on diabatic surfaces (here, they are RP and GS), μ_{12} is the transition dipole moment coupling the adiabatic surfaces of the ground and excited states, and $\Delta\mu_{12}$, the change in dipole moment between the ground (μ_1) and excited

 (μ_2) states where 1 and 2 represent each state on adiabatic surfaces. $\Delta \mu_{ab}$ and $\Delta \mu_{12}$ are related to the diabatic and adiabatic electron transfer distance through $d_{ab} \equiv \Delta \mu_{ab}/e$ and $d_{12} \equiv \Delta \mu_{12}/e$. We can apply GMH to an arbitrary nuclear geometry. 94-95 Here, we used the optimized GS and the optimized RP state within TDDFT. We used B3LYP/6-31G(d)/PCM (CHCl₃), which correctly predicts the nature of RP (BDH•-Bridge-TPA•+, please see Supporting Information, Figure S9) as the lowest charge-separated state or RP state whose energy is lower than S1BD* and higher than T1BD* at the GS geometries. A long-range corrected functional (CAM-B3LYP and ωB97XD) incorrectly placed the RP state energetically higher than S1BD* while another hybrid functional PBEPBE correctly places the RP state lower than S1BD* but incorrectly places it lower than ^{T1}BD* as well (Supporting Information, Table S3). The difficulty of modeling longrange charge-transfer excited states by TDDFT is well recognized, 96 and very recently Forde, Tretiak and co-workers⁹⁷ examined one of our D-B-A compounds, ¹³ showing that state-specific schemes⁹⁸ can more accurately describe solvation induced stabilization of RP states. Their approach may prove useful in future studies. ΔE is defined as the vertical energy gap at each reaction coordinate. We only consider the x- component of all dipole vectors which are aligned along a direction defined by the centroids of the D and A moieties; projecting μ_{12} along the electron transfer direction. The GMH analysis (with B3LYP functional) provided us with $V_{\rm DA}$ values that are comparable to those obtained by the radiative decay approach (Table 3). We obtained similar but slightly smaller V_{DA} values with PBEPBE functional (Supporting Information, Table S4). While the coupling values depend on the geometries, ^{14, 99} they generally decrease with increasing $r_{\rm DA}$: notably it decreases by half for 3 compared to 1.

We also used eq. 4 (the semiclassical Marcus equation with electron-vibration coupling) with spectral λ_S and λ_V , which yielded about 2-3 times larger V_{DA} values compared to the radiative

decay and GMH analyses (Table 3): note that the use of λ 's from the Arrhenius/two-sphere yielded much larger values (>> 0.1 eV). The semiclassical Marcus equation assumes that the ET reactions are nonadiabatic, 100 although, for electronic couplings larger than \sim 200 cm⁻¹, 6 , 101 the reactions may have significant adiabatic character and therefore becomes less dependent on V_{DA} . A simple analysis based on the Landau-Zerner expression 100 indicates that ET reactions, especially in 1, may well be in the adiabatic regime.

While our current analyses are admittedly not complete, all the analyses showed an expected distance dependence of the electronic couplings within the series (Supporting Information, Figure S9). Yet, the distance-dependent change in solvent reorganization energies is significant enough to accelerate the nonradiative charge recombination process in the Marcus inverted region. As shown in Figure 6, even with expected and observed decrease in V_{DA} with increasing r_{DA} , the Marcus curves shift down and to the right, creating a regime in the inverted region where k_{CRS} is faster at larger r_{DA} .

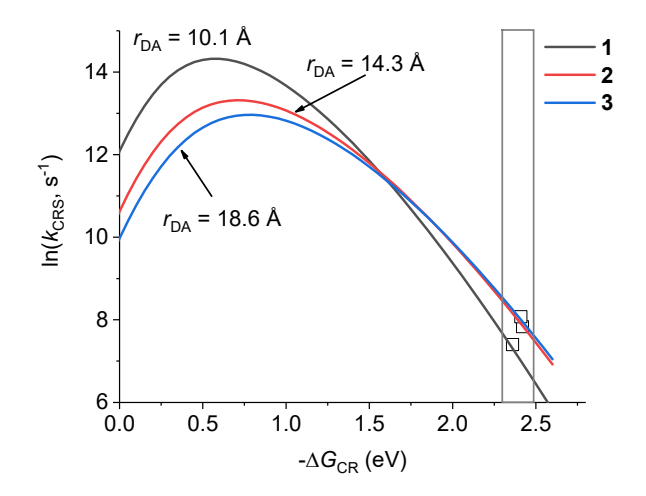


Figure 6. Gibbs energy dependence of singlet charge recombination rates (k_{CRS}) at three different donor–acceptor distances (r_{DA}). The solid lines are calculated using eq. 4 with λ values obtained from fittings of the CT emission spectra. V_{DA} are 880, 300, and 200 cm⁻¹ for 1, 2, and 3, respectively. The box highlights the data points of experimentally measured k_{CRS} .

5. Conclusions

We presented a new series of D-B-A systems with a kinked bridge group. A series of evidence was presented to unambiguously support the formation of the RP state and the presence of CT emission. Despite the kink between the donor and acceptor, in the form of mesosubstitutions, the electronic coupling constant was not significantly reduced to prevent the formation of RP states, but the quantum yields of CT emission were lower than those in the perpendicular motif. 13. Unexpectedly, a trend was recognized in the series of k_{CRS} increasing with r_{DA} . This trend was understood to be due to the distance dependence λ_S . Kuss-Petermann and Wenger³¹⁻³² observed the same trend, attributing to the sharp distance dependent λs and almost distance independent $V_{\rm DA}$. Taking advantage of the existence of radiative decay, we estimated λ s experimentally from the analysis of CT emission spectra and were able to show that λ s increases with increasing r_{DA} . On the other hand, unlike examples by Kuss-Petermann and Wenger, our analysis showed that V_{DA} decrease with increasing r_{DA} , but λ_S increases with r_{DA} at such a rate it offsets the decrease of $V_{\rm DA}$ to result in faster $k_{\rm CRS}$. With this work, we provide further evidence that λ_s increasing with r_{DA} results in k_{ET} increasing even when V_{DA} has expected to decrease with distance. While we could provide some quantification, our current analysis is not complete and further work is still needed for a more complete understanding of these observations. Yet, with the underlying connections between nonradiative and radiative decays, we showed that the existence and analysis of radiative charge recombination can provide much needed quantitative information on this underexplored effect. Such a fundamental understanding will aid us in the synthetic regulation of ET reactions and in developing optically addressable, specifically based on emission, molecular qubits with SCRPs.

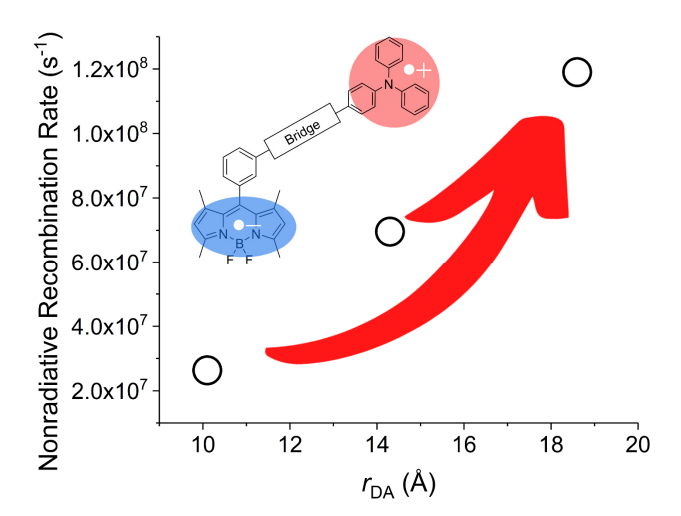
ASSOCIATED CONTENT

Supporting Information. The following files are available free of charge. Experimental methods, characterizations of new compounds, Figures S1-9, Tables S1-4, and reference.

ACKNOWLEDGMENT

The author acknowledges funding by the National Science Foundation under Grant No. 2144787, an NSF CAREER Award and partly by JST, PRESTO Grant Number JPMJPR17GA.

TOC Graphic



REFERENCES

- 1. Blankenship, R. E., *Molecular mechanisms of photosynthesis*. Blackwell Science: Oxford, 2002.
- 2. S G Boxer; C E D Chidsey, a.; Roelofs, M. G. Magnetic Field Effects on Reaction Yields in the Solid State: An Example from Photosynthetic Reaction Centers. *Annu. Rev. Phys. Chem.* **1983**, *34*, 389-417.
- 3. Wasielewski, M. R. Energy, charge, and spin transport in molecules and self-assembled nanostructures inspired by photosynthesis. *J. Org. Chem.* **2006,** *71*, 5051-5066.
- 4. Gust, D.; Moore, T. A.; Moore, A. L. Solar Fuels via Artificial Photosynthesis. *Accounts Chem. Res.* **2009**, *42*, 1890-1898.
- 5. Berardi, S.; Drouet, S.; Francas, L.; Gimbert-Surinach, C.; Guttentag, M.; Richmond, C.; Stoll, T.; Llobet, A. Molecular artificial photosynthesis. *Chem. Soc. Rev.* **2014**, *43*, 7501-7519.
- 6. Closs, G. L.; Miller, J. R. Intramolecular Long-Distance Electron Transfer in Organic Molecules. *Science* **1988**, *240*, 440-447.
- 7. Wasielewski, M. R. Photoinduced Electron Transfer in Supramolecular Systems for Artificial Photosynthesis. *Chem. Rev.* **1992,** *92*, 435-461.
- 8. Verhoeven, J. W. On the role of spin correlation in the formation, decay, and detection of long-lived, intramolecular charge-transfer states. *J. Photochem. Photobiol. C* **2006,** *7*, 40-60.
- 9. Wasielewski, M. R.; Forbes, M. D. E.; Frank, N. L.; Kowalski, K.; Scholes, G. D.; Yuen-Zhou, J.; Baldo, M. A.; Freedman, D. E.; Goldsmith, R. H.; Goodson, T., et al. Exploiting chemistry and molecular systems for quantum information science. *Nat. Rev. Chem.* **2020**, *4*, 490-504.
- 10. Harvey, S. M.; Wasielewski, M. R. Photogenerated Spin-Correlated Radical Pairs: From Photosynthetic Energy Transduction to Quantum Information Science. *J. Am. Chem. Soc.* **2021**, *143*, 15508-15529.
- 11. Mani, T. Molecular qubits based on photogenerated spin-correlated radical pairs for quantum sensing. *Chem. Phys. Rev.* **2022**, *3*, 021301.
- 12. Pasman, P.; Rob, F.; Verhoeven, J. W. Intramolecular charge-transfer absorption and emission resulting from through-bond interaction in bichromophoric molecules. *J. Am. Chem. Soc.* **1982**, *104*, 5127-5133.

- 13. Buck, J. T.; Wilson, R. W.; Mani, T. Intramolecular Long-Range Charge-Transfer Emission in Donor–Bridge–Acceptor Systems. *J. Phys. Chem. Lett.* **2019**, *10*, 3080-3086.
- 14. Buck, J. T.; Mani, T. Magnetic Control of Recombination Fluorescence and Tunability by Modulation of Radical Pair Energies in Rigid Donor–Bridge–Acceptor Systems. *J. Am. Chem. Soc.* **2020**, *142*, 20691-20700.
- 15. Loew, L. M. Design and characterization of electrochromic membrane probes. *J. Biochem. Biophys. Methods* **1982**, *6*, 243-260.
- 16. Uoyama, H.; Goushi, K.; Shizu, K.; Nomura, H.; Adachi, C. Highly efficient organic light-emitting diodes from delayed fluorescence. *Nature* **2012**, *492*, 234-238.
- 17. Miller, E. W. Small Molecule Fluorescent Voltage Indicators for Studying Membrane Potential. *Curr. Opin. Chem. Biol.* **2016,** *33*, 74-80.
- 18. Fang, Q.; Li, J.; Li, S.; Duan, R.; Wang, S.; Yi, Y.; Guo, X.; Qian, Y.; Huang, W.; Yang, G. Thermally populated "bright" states for wide-range and high temperature sensing in air. *Chem. Commun.* **2017**, *53*, 5702-5705.
- 19. Gomez-Bombarelli, R.; Aguilera-Iparraguirre, J.; Hirzel, T. D.; Duvenaud, D.; Maclaurin, D.; Blood-Forsythe, M. A.; Chae, H. S.; Einzinger, M.; Ha, D.-G.; Wu, T., et al. Design of efficient molecular organic light-emitting diodes by a high-throughput virtual screening and experimental approach. *Nat. Mater.* **2016**, *15*, 1120-1127.
- 20. Tsujimoto, H.; Ha, D.-G.; Markopoulos, G.; Chae, H. S.; Baldo, M. A.; Swager, T. M. Thermally Activated Delayed Fluorescence and Aggregation Induced Emission with Through-Space Charge Transfer. *J. Am. Chem. Soc.* **2017**, *139*, 4894-4900.
- 21. Oosterbaan, W. D.; Koper, C.; Braam, T. W.; Hoogesteger, F. J.; Piet, J. J.; Jansen, B. A. J.; van Walree, C. A.; van Ramesdonk, H. J.; Goes, M.; Verhoeven, J. W., et al. Oligo(Cyclohexylidene)s and Oligo(Cyclohexyl)s as Bridges for Photoinduced Intramolecular Charge Separation and Recombination. *J. Phys. Chem. A* **2003**, *107*, 3612-3624.
- 22. Oevering, H.; Verhoeven, J. W.; Paddon-Row, M. N.; Warman, J. M. Charge-transfer absorption and emission resulting from long-range through-bond interaction; exploring the relation between electronic coupling and electron-transfer in bridged donor-acceptor systems. *Tetrahedron* **1989**, *45*, 4751-4766.
- 23. Oevering, H.; Paddon-Row, M. N.; Heppener, M.; Oliver, A. M.; Cotsaris, E.; Verhoeven, J. W.; Hush, N. S. Long-range photoinduced through-bond electron transfer and

- radiative recombination via rigid nonconjugated bridges: distance and solvent dependence. *J. Am. Chem. Soc.* **1987,** *109*, 3258-3269.
- 24. Murrell, J. N. Molecular Complexes and their Spectra. IX. The Relationship between the Stability of a Complex and the Intensity of its Charge-transfer Bands1. *J. Am. Chem. Soc.* **1959**, *81*, 5037-5043.
- 25. Bixon, M.; Jortner, J.; Verhoeven, J. W. Lifetimes for Radiative Charge Recombination in Donor-Acceptor Molecules. *J. Am. Chem. Soc.* **1994**, *116*, 7349-7355.
- 26. Klein, J. H.; Schmidt, D.; Steiner, U. E.; Lambert, C. Complete Monitoring of Coherent and Incoherent Spin Flip Domains in the Recombination of Charge-Separated States of Donor-Iridium Complex-Acceptor Triads. *J. Am. Chem. Soc.* **2015**, *137*, 11011-11021.
- 27. Kimoto, K.; Satoh, T.; Iwamura, M.; Nozaki, K.; Horikoshi, T.; Suzuki, S.; Kozaki, M.; Okada, K. Very Long-Lived Photoinduced Charge-Separated States of Triphenylamine—Naphthalenediimide Dyads in Polymer Matrices. *J. Phys. Chem. A* **2016**, *120*, 8093-8103.
- 28. Werner, U.; Sakaguchi, Y.; Hayashi, H.; Nohya, G.; Yoneshima, R.; Nakajima, S.; Osuka, A. Magnetic field effects in the radical ion pair recombination of fixed-distance triads consisting of porphyrins and an electron acceptor. *J. Phys. Chem.* **1995**, *99*, 13930-13937.
- 29. Gorczak, N.; Renaud, N.; Tarkuç, S.; Houtepen, A. J.; Eelkema, R.; Siebbeles, L. D. A.; Grozema, F. C. Charge transfer versus molecular conductance: molecular orbital symmetry turns quantum interference rules upside down. *Chem. Sci.* **2015**, *6*, 4196-4206.
- 30. Brunschwig, B. S.; Ehrenson, S.; Sutin, N. The distance dependence of electron transfer reactions: rate maxima and rapid rates at large reactant separations. *J. Am. Chem. Soc.* **1984**, *106*, 6858-6859.
- 31. Kuss-Petermann, M.; Wenger, O. S. Increasing Electron-Transfer Rates with Increasing Donor–Acceptor Distance. *Angew. Chem. Int. Edit.* **2016**, *55*, 815-819.
- 32. Kuss-Petermann, M.; Wenger, O. S. Electron Transfer Rate Maxima at Large Donor–Acceptor Distances. *J. Am. Chem. Soc.* **2016**, *138*, 1349-1358.
- 33. Kuss-Petermann, M.; Wenger, O. S. Unusual distance dependences of electron transfer rates. *Phys. Chem. Chem. Phys.* **2016**, *18*, 18657-18664.
- 34. Luo, Y.; Barthelmes, K.; Wächtler, M.; Winter, A.; Schubert, U. S.; Dietzek, B. Increased Charge Separation Rates with Increasing Donor–Acceptor Distance in Molecular Triads: The Effect of Solvent Polarity. *J. Phys. Chem. C* **2017**, *121*, 9220-9229.

- 35. Carmichael, I.; Hug, G. L. Triplet–Triplet Absorption Spectra of Organic Molecules in Condensed Phases. *J. Phys. Chem. Ref. Data* **1986,** *15*, 1-250.
- 36. Buck, J. T.; Boudreau, A. M.; DeCarmine, A.; Wilson, R. W.; Hampsey, J.; Mani, T. Spin-Allowed Transitions Control the Formation of Triplet Excited States in Orthogonal Donor-Acceptor Dyads. *Chem* **2019**, *5*, 138-155.
- 37. Frisch, M. J.; Trucks, G. W.; Schlegel, H. B.; Scuseria, G. E.; Robb, M. A.; Cheeseman, J. R.; Scalmani, G.; Barone, V.; Petersson, G. A.; Nakatsuji, H., et al. *Gaussian 16 Rev. B.01*, Wallingford, CT, 2016.
- 38. Becke, A. D. Density-Functional Thermochemistry. III. The Role of Exact Exchange. *J. Chem. Phys.* **1993**, *98*, 5648-5652.
- 39. Stephens, P. J.; Devlin, F. J.; Chabalowski, C. F.; Frisch, M. J. Ab-Initio Calculation of Vibrational Absorption and Circular-Dichroism Spectra Using Density-Functional Force-Fields. *J. Phys. Chem.* **1994**, *98*, 11623-11627.
- 40. Perdew, J. P.; Burke, K.; Ernzerhof, M. Generalized Gradient Approximation Made Simple. *Phys. Rev. Lett.* **1996,** 77, 3865-3868.
- 41. Perdew, J. P.; Burke, K.; Ernzerhof, M. Generalized Gradient Approximation Made Simple [Phys. Rev. Lett. 77, 3865 (1996)]. *Phys. Rev. Lett.* **1997,** 78, 1396-1396.
- 42. Yanai, T.; Tew, D. P.; Handy, N. C. A new hybrid exchange-correlation functional using the Coulomb-attenuating method (CAM-B3LYP). *Chem. Phys. Lett.* **2004**, *393*, 51-57.
- 43. Chai, J.-D.; Head-Gordon, M. Long-range corrected hybrid density functionals with damped atom-atom dispersion corrections. *Phys. Chem. Chem. Phys.* **2008**, *10*, 6615-6620.
- 44. Improta, R.; Scalmani, G.; Frisch, M. J.; Barone, V. Toward effective and reliable fluorescence energies in solution by a new state specific polarizable continuum model time dependent density functional theory approach. *J. Chem. Phys.* **2007**, *127*, 074504 074501-074509.
- 45. Improta, R.; Barone, V.; Scalmani, G.; Frisch, M. J. A state-specific polarizable continuum model time dependent density functional theory method for excited state calculations in solution. *J. Chem. Phys.* **2006**, *125*, 054103 054101-054109.
- 46. Tomasi, J.; Mennucci, B.; Cammi, R. Quantum Mechanical Continuum Solvation Models. *Chem. Rev.* **2005**, *105*, 2999-3094.

- 47. Oka, N.; Yamada, T.; Sajiki, H.; Akai, S.; Ikawa, T. Aryl Boronic Esters Are Stable on Silica Gel and Reactive under Suzuki–Miyaura Coupling Conditions. *Org. Lett.* **2022**, *24*, 3510-3514.
- 48. Ziessel, R.; Ulrich, G.; Harriman, A. The chemistry of Bodipy: a new El Dorado for fluorescence tools. *New. J. Chem.* **2007**, *31*, 496-501.
- 49. Loudet, A.; Burgess, K. BODIPY dyes and their derivatives: Syntheses and spectroscopic properties. *Chem. Rev.* **2007**, *107*, 4891-4932.
- 50. Bergström, F.; Mikhalyov, I.; Hägglöf, P.; Wortmann, R.; Ny, T.; Johansson, L. B. Å. Dimers of Dipyrrometheneboron Difluoride (BODIPY) with Light Spectroscopic Applications in Chemistry and Biology. *J. Am. Chem. Soc.* **2002**, *124*, 196-204.
- 51. Tian, L.; Feiwu, C. Multiwfn: A multifunctional wavefunction analyzer. *J. Comput. Chem.* **2012**, *33*, 580-592.
- 52. Guido, C. A.; Cortona, P.; Mennucci, B.; Adamo, C. On the Metric of Charge Transfer Molecular Excitations: A Simple Chemical Descriptor. *J. Chem. Theory Comput.* **2013**, *9*, 3118-3126.
- 53. Lor, M.; Thielemans, J.; Viaene, L.; Cotlet, M.; Hofkens, J.; Weil, T.; Hampel, C.; Müllen, K.; Verhoeven, J. W.; Van der Auweraer, M., et al. Photoinduced Electron Transfer in a Rigid First Generation Triphenylamine Core Dendrimer Substituted with a Peryleneimide Acceptor. *J. Am. Chem. Soc.* **2002**, *124*, 9918-9925.
- 54. Zimmt, M. B.; Waldeck, D. H. Exposing Solvent's Roles in Electron Transfer Reactions: Tunneling Pathway and Solvation. *J. Phys. Chem. A* **2003**, *107*, 3580-3597.
- 55. Chi, C.; Wegner, G. Chain-Length Dependence of the Electrochemical Properties of Conjugated Oligofluorenes. *Macromol. Rapid Comm.* **2005**, *26*, 1532-1537.
- 56. Zaikowski, L.; Kaur, P.; Gelfond, C.; Selvaggio, E.; Asaoka, S.; Wu, Q.; Chen, H.-C.; Takeda, N.; Cook, A. R.; Yang, A., et al. Polarons, Bipolarons, and Side-By-Side Polarons in Reduction of Oligofluorenes. *J. Am. Chem. Soc.* **2012**, *134*, 10852-10863.
- 57. Hapiot, P.; Lagrost, C.; Le Floch, F.; Raoult, E.; Rault-Berthelot, J. Comparative Study of the Oxidation of Fluorene and 9,9-Disubstituted Fluorenes and Their Related 2,7'-Dimers and Trimer. *Chem. Mater.* **2005**, *17*, 2003-2012.

- 58. Merkel, P. B.; Luo, P.; Dinnocenzo, J. P.; Farid, S. Accurate Oxidation Potentials of Benzene and Biphenyl Derivatives via Electron-Transfer Equilibria and Transient Kinetics. *J. Org. Chem.* **2009**, *74*, 5163-5173.
- 59. Baleizão, C.; Berberan-Santos, M. N. Thermally activated delayed fluorescence as a cycling process between excited singlet and triplet states: Application to the fullerenes. *J. Chem. Phys.* **2007**, *126*, 204510.
- 60. Steiner, U. E.; Ulrich, T. Magnetic-Field Effects in Chemical-Kinetics and Related Phenomena. *Chem. Rev.* **1989**, *89*, 51-147.
- 61. Scott, A. M.; Wasielewski, M. R. Temperature Dependence of Spin-Selective Charge Transfer Pathways in Donor–Bridge–Acceptor Molecules with Oligomeric Fluorenone and p-Phenylethynylene Bridges. *J. Am. Chem. Soc.* **2011**, *133*, 3005-3013.
- 62. Barbara, P. F.; Meyer, T. J.; Ratner, M. A. Contemporary Issues in Electron Transfer Research. *J. Phys. Chem.* **1996**, *100*, 13148-13168.
- 63. Sukegawa, J.; Schubert, C.; Zhu, X. Z.; Tsuji, H.; Guldi, D. M.; Nakamura, E. Electron transfer through rigid organic molecular wires enhanced by electronic and electron-vibration coupling. *Nat. Chem.* **2014**, *6*, 899-905.
- 64. Yonemoto, E. H.; Saupe, G. B.; Schmehl, R. H.; Hubig, S. M.; Riley, R. L.; Iverson, B. L.; Mallouk, T. E. Electron-Transfer Reactions of Ruthenium Trisbipyridyl-Viologen Donor-Acceptor Molecules: Comparison of the Distance Dependence of Electron Transfer-Rates in the Normal and Marcus Inverted Regions. *J. Am. Chem. Soc.* **1994**, *116*, 4786-4795.
- 65. Tachiya, M.; Murata, S. New explanation for the lack of the inverted region in charge separation reactions. *J. Phys. Chem.* **1992**, *96*, 8441-8444.
- 66. Marcus, R. A. Chemical and Electrochemical Electron-Transfer Theory. *Annu. Rev. Phys. Chem.* **1964**, *15*, 155-196.
- 67. Myers, A. B. Resonance Raman Intensities and Charge-Transfer Reorganization Energies. *Chem. Rev.* **1996**, *96*, 911-926.
- 68. Isied, S. S.; Vassilian, A.; Wishart, J. F.; Creutz, C.; Schwarz, H. A.; Sutin, N. The distance dependence of intramolecular electron-transfer rates: importance of the nuclear factor. *J. Am. Chem. Soc.* **1988**, *110*, 635-637.

- 69. Vath, P.; Zimmt, M. B.; Matyushov, D. V.; Voth, G. A. A Failure of Continuum Theory: Temperature Dependence of the Solvent Reorganization Energy of Electron Transfer in Highly Polar Solvents. *J. Phys. Chem. B* **1999**, *103*, 9130-9140.
- 70. Matyushov, D. V. Energetics of Electron-Transfer Reactions in Soft Condensed Media. *Accounts Chem. Res.* **2007**, *40*, 294-301.
- 71. Matyushov, D. V.; Voth, G. A. A perturbation theory for solvation thermodynamics: Dipolar–quadrupolar liquids. *J. Chem. Phys.* **1999**, *111*, 3630-3638.
- 72. Kumar, K.; Lin, Z.; Waldeck, D. H.; Zimmt, M. B. Electronic Coupling in C-Clamp-Shaped Molecules: Solvent-Mediated Superexchange Pathways. *J. Am. Chem. Soc.* **1996**, *118*, 243-244.
- 73. Marcus, R. A. On Theory of Electron-Transfer Reactions .6. Unified Treatment for Homogeneous and Electrode Reactions. *J. Chem. Phys.* **1965**, *43*, 679-&.
- 74. Hush, N. S. Homogeneous and Heterogeneous Optical and Thermal Electron Transfer. *Electrochim. Acta* **1968**, *13*, 1005-1023.
- 75. Marcus, R. A. Relation between charge transfer absorption and fluorescence spectra and the inverted region. *J. Phys. Chem.* **1989**, *93*, 3078-3086.
- 76. Bixon, M.; Jortner, J., Electron Transfer—from Isolated Molecules to Biomolecules. In *Advances in Chemical Physics*, 1999; Vol. 106, pp 35-202.
- 77. Gould, I. R.; Noukakis, D.; Goodman, J. L.; Young, R. H.; Farid, S. A quantitative relationship between radiative and nonradiative electron transfer in radical-ion pairs. *J. Am. Chem. Soc.* **1993**, *115*, 3830-3831.
- 78. Gould, I. R.; Young, R. H.; Moody, R. E.; Farid, S. Contact and solvent-separated geminate radical ion pairs in electron-transfer photochemistry. *J. Phys. Chem.* **1991**, *95*, 2068-2080.
- 79. Kumar, K.; Kurnikov, I. V.; Beratan, D. N.; Waldeck, D. H.; Zimmt, M. B. Use of Modern Electron Transfer Theories To Determine Electronic Coupling Matrix Elements in Intramolecular Systems. *J. Phys. Chem. A* **1998**, *102*, 5529-5541.
- 80. Vath, P.; Zimmt, M. B. A Spectroscopic Study of Solvent Reorganization Energy: Dependence on Temperature, Charge Transfer Distance, and the Type of Solute–Solvent Interactions. *J. Phys. Chem. A* **2000**, *104*, 2626-2633.

- 81. Cortes, J.; Heitele, H.; Jortner, J. Band-shape analysis of the charge-transfer fluorescence in barrelene-based electron donor-acceptor compounds. *J. Phys. Chem.* **1994**, *98*, 2527-2536.
- 82. Marcus, R. A. On the Theory of Oxidation-Reduction Reactions Involving Electron Transfer .1. *J. Chem. Phys.* **1956**, *24*, 966-978.
- 83. Jortner, J. Temperature dependent activation energy for electron transfer between biological molecules. *J. Chem. Phys.* **1976**, *64*, 4860-4867.
- 84. Miller, J. R.; Beitz, J. V.; Huddleston, R. K. Effect of free energy on rates of electron transfer between molecules. *J. Am. Chem. Soc.* **1984,** *106*, 5057-5068.
- 85. Osuka, A.; Noya, G.; Taniguchi, S.; Okada, T.; Nishimura, Y.; Yamazaki, I.; Mataga, N. Energy-Gap Dependence of Photoinduced Charge Separation and Subsequent Charge Recombination in 1,4-Phenylene-Bridged Zinc-Free-Base Hybrid Porphyrins. *Chem. Eur. J.* **2000,** *6*, 33-46.
- 86. Waskasi, M. M.; Kodis, G.; Moore, A. L.; Moore, T. A.; Gust, D.; Matyushov, D. V. Marcus Bell-Shaped Electron Transfer Kinetics Observed in an Arrhenius Plot. *J. Am. Chem. Soc.* **2016**, *138*, 9251-9257.
- 87. Mulliken, R. S. Molecular Compounds and their Spectra. II. *J. Am. Chem. Soc.* **1952,** *74*, 811-824.
- 88. Gould, I. R.; Young, R. H.; Mueller, L. J.; Albrecht, A. C.; Farid, S. Electronic Coupling Matrix Elements in Acceptor-Donor Excited States and the Effect of Charge-Transfer Character on Their Radiative Rate Constants. *J. Am. Chem. Soc.* **1994**, *116*, 3147-3148.
- 89. Gould, I. R.; Young, R. H.; Mueller, L. J.; Albrecht, A. C.; Farid, S. Electronic-Structures of Exciplexes and Excited Charge-Transfer Complexes. *J. Am. Chem. Soc.* **1994**, *116*, 8188-8199.
- 90. Gould, I. R.; Noukakis, D.; Gomez-Jahn, L.; Goodman, J. L.; Farid, S. Explanation of the driving-force dependence of return electron transfer in contact radical-ion pairs. *J. Am. Chem. Soc.* **1993**, *115*, 4405-4406.
- 91. Armaroli, N.; Accorsi, G.; Song, F.; Palkar, A.; Echegoyen, L.; Bonifazi, D.; Diederich, F. Photophysical and Electrochemical Properties of meso, meso-Linked Oligoporphyrin Rods with Appended Fullerene Terminals. *Chemphyschem* **2005**, *6*, 732-743.

- 92. Kang, Y. K.; Zhang, P.; Rubtsov, I. V.; Zheng, J.; Bullard, G.; Beratan, D. N.; Therien, M. J. Orientational Dependence of Cofacial Porphyrin–Quinone Electronic Interactions within the Strong Coupling Regime. *J. Phys. Chem. B* **2019**, *123*, 10456-10462.
- 93. Zheng, J.; Kang, Y. K.; Therien, M. J.; Beratan, D. N. Generalized Mulliken–Hush Analysis of Electronic Coupling Interactions in Compressed π-Stacked Porphyrin–Bridge–Quinone Systems. *J. Am. Chem. Soc.* **2005**, *127*, 11303-11310.
- 94. Cave, R. J.; Newton, M. D. Generalization of the Mulliken-Hush treatment for the calculation of electron transfer matrix elements. *Chem. Phys. Lett.* **1996**, *249*, 15-19.
- 95. Cave, R. J.; Newton, M. D. Calculation of electronic coupling matrix elements for ground and excited state electron transfer reactions: Comparison of the generalized Mulliken-Hush and block diagonalization methods. *J. Chem. Phys.* **1997**, *106*, 9213-9226.
- 96. Dreuw, A.; Head-Gordon, M. Failure of Time-Dependent Density Functional Theory for Long-Range Charge-Transfer Excited States: The Zincbacteriochlorin–Bacteriochlorin and Bacteriochlorophyll–Spheroidene Complexes. *J. Am. Chem. Soc.* **2004**, *126*, 4007-4016.
- 97. Forde, A.; Freixas, V. M.; Fernandez-Alberti, S.; Neukirch, A. J.; Tretiak, S. Charge-Transfer Luminescence in a Molecular Donor–Acceptor Complex: Computational Insights. *J. Phys. Chem. Lett.* **2022**, *13*, 8755-8760.
- 98. Bjorgaard, J. A.; Kuzmenko, V.; Velizhanin, K. A.; Tretiak, S. Solvent effects in time-dependent self-consistent field methods. I. Optical response calculations. *J. Chem. Phys.* **2015**, *142*, 044103.
- 99. Yang, X.; Keane, T.; Delor, M.; Meijer, A. J. H. M.; Weinstein, J.; Bittner, E. R. Identifying electron transfer coordinates in donor-bridge-acceptor systems using mode projection analysis. *Nat. Commun.* **2017**, *8*, 14554.
- 100. Newton, M. D. Quantum Chemical Probes of Electron-Transfer Kinetics the Nature of Donor-Acceptor Interactions. *Chem. Rev.* **1991**, *91*, 767-792.
- 101. Burghart, A.; Kim, H.; Welch, M. B.; Thoresen, L. H.; Reibenspies, J.; Burgess, K.; Bergström, F.; Johansson, L. B. Å. 3,5-Diaryl-4,4-difluoro-4-bora-3a,4a-diaza-s-indacene (BODIPY) Dyes: Synthesis, Spectroscopic, Electrochemical, and Structural Properties. *J. Org. Chem.* **1999**, *64*, 7813-7819.